International Journal of Computer Trends and Technology
ISSN: 2231–2803 / https://doi.org/10.14445/22312803/IJCTT-V73I8P105

Volume 73 Issue 8, 33-40, August 2025

Original Article

Physically Transparent LBL Modeling of 0.3–1 THz Attenuation: Windowed Foreign-Continuum Scaling and Validation

Ahmed Sidi Aman[1], Ramafiarisona Hajasoa Malala[2]

[1,2] *STII TASI, University of Antananarivo, Madagascar.*

Corresponding Author : engineer.sidi@gmail.com

Received: 15 June 2025 Revised: 23 July 2025 Accepted: 15 August 2025 Published: 30 August 2025

Abstract - *This study presents a modular Line-By-Line (LBL) model for atmospheric attenuation over the 0.3–1 THz band, separating spectral lines (from HITRAN with exact Voigt evaluation), water-vapor continuum components (MT_CKD 4.3, independently reading self and foreign terms), and dry-air collision-induced absorption (from N_2/O_2). The computational workflow mirrors a reference FTS setup in MATLAB, including high-resolution spectra, 3-GHz transmission binning, and recovery of α. During validation with an independent FTS dataset, the uncorrected LBL model shows a consistent underestimation in specific valley regions, though line peaks remain accurately captured. To mitigate this bias, a frequency-dependent foreign-only scaling S(f) is applied—affine in frequency, smoothly windowed between 600–980 GHz, with damping γ = 0.60 and a dominance rule to limit misapplication. Tested across four humidity scenarios, the corrected model significantly reduces valley errors—most notably between 800–900 GHz—yielding MAE reductions of 50–90% in the Z5 window and pulling local biases closer to zero. Band-averaged metrics improve more modestly (around 2–3%) due to unchanged peaks. Under the tested conditions, the dry background remains negligible and does not explain the offset. In link-budget terms, compensating this valley bias improves margin reliability in usable windows by several tens of dB/km. The resulting LBL×S(f) model thus offers a clear, effective framework for planning high-capacity THz links.*

Keywords - *Atmospheric attenuations, Continuum scalings, Line-By-Line models, Terahertz links, Water-vapor continuum models.*

1. Introduction

Ultra–high–throughput wireless links at terahertz (THz, ~0.1–10 THz) rely on spectral "windows" that are relatively transparent in the atmospheric channel. In prior work, the groundwork for THz link dimensioning was laid by relying on engineering reference models and on experimental comparisons that enabled the refinement of five windows over the 0.3–1 THz band. However, to size a credible link budget, it is not enough to invoke an aggregated model: it is necessary to understand how each physical brick contributes to loss, particularly the background between spectral lines (continuum).

The ITU-R P.676 recommendations [1] or proven radiative codes (e.g., AM) [2] are excellent global comparison points, but their "black-box" nature limits mechanistic analysis and the ability to isolate the part that explains local discrepancies in valleys. While radiative-transfer tools such as LBLRTM and AM are extensively documented, their workflows are not typically structured for modular examination of THz-scale communication links—especially with emphasis on spectral valleys. This gap implies a need for a spectrally decomposable LBL framework whose structure corresponds directly to THz link budgets and enables inspection of local deviations in transparent windows.

This article is a direct continuation of that approach: it aims to equip THz analysis with a decomposable Line-By-Line (LBL) model, designed to go into detail and connect each physical contribution to discrepancies observed within windows useful for communications. This step is a methodological milestone toward a fully controlled link budget, which will be the subject of future work.

This work contributes two interrelated elements: a fully documented academic LBL implementation tailored to the 0.3–1 THz band, and a spectrally windowed scaling function S(f) applied solely to the foreign-continuum component to reconcile valley-scale model-measurement differences.

The proposed LBL explicitly separates the following contributions, aligning with the implemented computation chain:

Discrete spectral lines modeled using the HITRAN database with exact Voigt profile evaluation to capture the fine structure of resonances. The water-vapor continuum, which is treated as the sum of self- and foreign-broadened absorption, following the MT_CKD 4.3 model with independent handling of each component, and dry-air background absorption, arising from collision-induced effects primarily involving nitrogen and oxygen pairs.

This modular breakdown allows us to isolate how each physical mechanism influences the observed attenuation, especially in spectral valleys where bulk models tend to diverge from experimental data. The model architecture is designed to match a high-resolution reference protocol based on Fourier transform spectroscopy (FTS) in MATLAB, enabling a direct reproduction of fine transmission spectra and consistent retrieval of absorption coefficients. By keeping all elements explicit and individually tunable, the LBL framework provides a transparent foundation for accuracy and interpretability—a key enabler for diagnosing and correcting mismatches in communication-relevant frequency bands.

Spectral lines from H_2O and O_2, including their isotopologues, are sourced from the HITRAN database. Line intensities Si(T) are computed using temperature-dependent partition functions Q(T) along with pressure- and temperature-broadened widths and line shifts. Each profile is evaluated using an exact Voigt formulation based on the Faddeeva function, ensuring a precise treatment of Doppler and collisional effects over the selected frequency grid.

- MT_CKD 4.3 water continuum: in two components read separately (self and foreign) from a driver NetCDF; these outputs are interpolated onto a grid, converted to absorption units α, and summed to the line term.
- "Dry air" background (CIA N_2/O_2): implemented in a closed form consistent with the engineering literature (the formulation used in practice in the defined MATLAB code), added in addition to oxygen lines to complete the non-aqueous background.

The numerical organization follows the reference instrumental protocol: a high-resolution spectral calculation, followed by 3-GHz binning in the transmission domain to replicate the FTS processing chain; absorption coefficients α are then obtained via the standard conversion −ln(T)/L, and values are interpolated smoothly using a shape-preserving (pchip) method along the measurement axis to enable consistent comparisons. The evaluation metrics—MAE, RMSE, and bias—are computed across the entire band as well as within specific spectral windows centered on valley regions of interest. Figure 1 outlines the model structure and validation pipeline, aligned with the FTS protocol: line absorption (from HITRAN, using exact Voigt profiles via the Faddeeva function), water-vapor continuum split into self and foreign terms, optional inclusion of dry-air CIA, and the final 3-GHz binning in the transmission domain prior to comparison with measurement data.

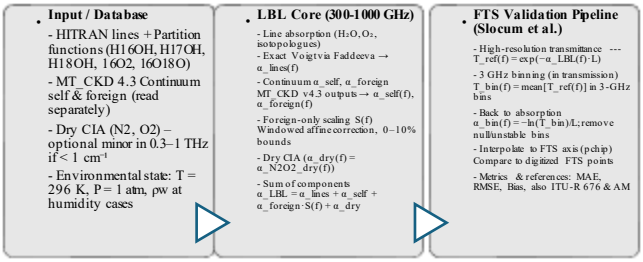

Fig. 1 Architecture of the decomposable LBL model and FTS validation chain (0.3-1 THz)

Finally, to probe the humid continuum without touching the micro-physics of the lines, an optional spectral factor S(f) is introduced and applied exclusively to the foreign component: S(f) is affine in frequency, windowed by a smoothed window (raised-cosine type) so as to act only in the band where analysis indicates it, and bounded to prevent any excess.

A local guardrail (criterion of dominance of the foreign component in the continuum) governs effective activation. The precise definition of S(f), of the frequency window, and of the bounds will be given in Methods, with the corresponding notations and unit conversions (HITRAN, Q(T), Voigt/Faddeeva, MT_CKD, dry CIA, 3-GHz binning).

2. Materials and Methods

The model is validated using the FTS dataset from Slocum et al. [3], which spans 300–1000 GHz under controlled conditions (cell length ≈ 4 m, temperature ≈ 296 K, pressure ≈ 1 atm) and includes four distinct humidity levels. To ensure consistency, their processing chain is replicated: high-resolution spectral calculation, 3-GHz binning in the transmission domain, recovery of α via the standard −ln T/L expression, and final interpolation using a pchip method aligned to the FTS measurement grid.

Evaluation metrics—MAE, RMSE, bias, and MAXE—are computed both across the full band and within specific valley-centered windows of interest. From a physical standpoint, when THz radiation propagates through humid air, the resulting spectral attenuation $\alpha(\tilde{\nu})$ reflects the influence of:

- sharp spectral lines, broadened by thermal and collisional effects;
- an underlying continuum between lines, arising from far-wing absorption and intermolecular interactions;
- a dry-air contribution (N_2/O_2), stemming from collision-induced dipole activity. To guide the analysis, Figure 2 maps the frequency range and marks the five spectral valleys used as design references for THz link planning.

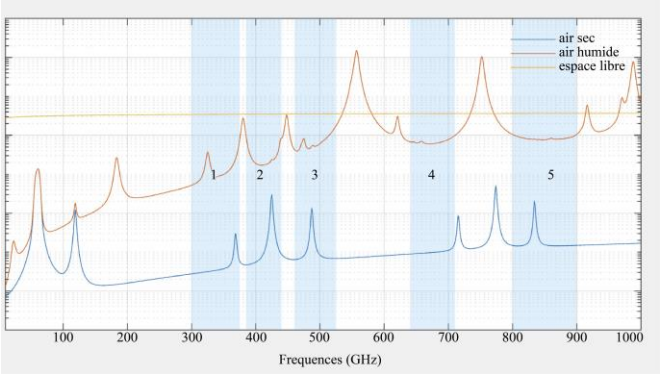

Fig. 2 Spectral landmarks over 0.3–1 THz and the 5 identified communication windows

The decomposable LBL isolates these bricks to properly attribute contributions:

$$\alpha(\tilde{\nu}) = \alpha_{\text{lines}}(\tilde{\nu}) + \underbrace{\alpha_{\text{self}}(\tilde{\nu}) + \alpha_{\text{foreign}}(\tilde{\nu})}_{\text{continuum } H_2O} + \alpha_{\text{dry}}(\tilde{\nu}).$$

2.1. Lines (HITRAN): data, broadenings, and Voigt/Faddeeva profile

HITRAN is a reference spectroscopic database [4] that provides, for each line and isotopologue, the parameters required for line-by-line evaluation: position $\tilde{\nu}$_i (or frequency), intensity $S_i(T_0)$ at (T_0=296 K, lower-state energy $E_{l,i}$), partition functions $Q(T)$, broadening coefficients (γ_{air}, γ_{self}), thermal exponent n, pressure shift δ_L, as well as relevant molecular masses. In the proposed LBL, these elements are used to build the population (via $Q(T)$ and $E_{l,i}$), the width and the spectral shape (profile) of each H_2O and O_2 line, including isotopologues.

2.1.1. Line Intensities (Temperature Dependence)

$$S_i(T) = S_i(T_0)\,\frac{Q(T_0)}{Q(T)}\,\exp\left[-c_2 E_{l,i}\left(\frac{1}{T}-\frac{1}{T_0}\right)\right]\frac{1-\exp(-c_2\tilde{\nu}_i/T)}{1-\exp(-c_2\tilde{\nu}_i/T_0)}, \qquad c_2 = \frac{hc}{k}.$$

Doppler

In air, molecules move at various speeds (temperature). A molecule coming toward the wave "sees" a slightly higher frequency, moving away, slightly lower. Because billions of molecules have different speeds, the resonance is not an infinitely thin line: it becomes a smooth hump around, $\tilde{\nu}_i$. Modeling (in wavenumber):

$$\Delta\tilde{\nu}_D = \tilde{\nu}_i\sqrt{\frac{2kT\ln 2}{mc^2}}, \qquad \sigma_G = \frac{\Delta\tilde{\nu}_D}{\sqrt{2\ln 2}}$$

Lorentz

Molecules bump into one another. Each collision interrupts the dipole oscillation a little, reducing its coherence time; this yields a frequency uncertainty and long tails: a Lorentzian profile. Broadening increases with pressure and depends on composition (water–water vs. water–air):

$$\gamma_L = \left[\gamma_{self}\,x + \gamma_{air}\,(1-x)\right]\frac{P}{P_0}\left(\frac{T_0}{T}\right)^n,$$

Where x is the H_2O mole fraction.

Figure 3 illustrates the individual Doppler and Lorentz contributions and their exact combination into a Voigt profile via the Faddeeva function.

Exact Voigt

In the real atmosphere, Doppler and collisions coexist near the center, the Gaussian (Doppler) component may dominate; in the wings, the Lorentzian (collisions) is important. The Voigt profile is the fusion of both and is evaluated with the Faddeeva function w(z) [5], which is numerically stable from core to wings (useful for the valley background):

$$\Phi_i(\tilde{\nu}) = \frac{\mathrm{Re}\{w(z)\}}{\sigma_G\sqrt{2\pi}}, \qquad z = \frac{(\tilde{\nu}-\tilde{\nu}_i) + i\,\gamma_L}{\sigma_G\sqrt{2}}.$$

$$\alpha_{\text{lines}}(\tilde{\nu}) = N_{\text{mol}}\sum_i S_i(T)\,\Phi_i(\tilde{\nu}),$$

Where N_{mol} is the molecular number density.

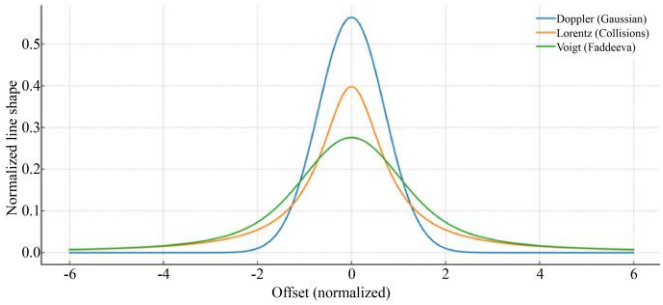

Fig. 3 Line-shape building blocks: Doppler, Lorentz, and exact Voigt (Faddeeva) on a representative transition

The exact Voigt evaluation avoids core/wing artifacts, which is essential when reading valley floors against the continuum.

2.2. H_2O continuum (MT_CKD 4.3): Definition, Separate Self/Foreign Reading, Conversions

Between resolved lines, one observes a smooth absorption due to the combined effect of far wings, collisional line mixing, and collision-induced correlations (induced dipoles, pairs/quasi-dimers). This completes the background set by line wings. In the FTS conditions, the decomposed analysis indicates that the H_2O continuum contributes a notable fraction to the valley floor, depending on humidity and frequency; the remainder mainly comes from H_2O line wings.

The dry background is minor here.

The self (H_2O–H_2O) and foreign (H_2O–air) components are read separately from an MT_CKD 4.3 driver NetCDF [6]. Two-unit cases:

- Cross-section $\sigma(\tilde{\nu})$ [cm²/molecule]:

$$\alpha(\tilde{\nu}) = N_0\,\sigma(\tilde{\nu}), N_0 = \frac{P_{H_2O}}{kT}\cdot\frac{1}{10^6}, P_{H_2O} = \frac{\rho_w}{1000}\,R_v\,T,$$

- Absorption [Np/cm]: convert Np/cm → dB/km via ($10\log_{10} e$) $\times 10^5$, then dB/km → m^{-1} by dividing by 4342.945. The total water continuum is

$$\alpha_{\text{cont},H_2O} = \alpha_{\text{self}} + \alpha_{\text{foreign}}$$

2.3. Dry-air background (CIA N_2/O_2): principle and closed-form expression

Collision-Induced Absorption (CIA) of the N_2/O_2 mixture reflects that transient dipoles appear during collisions, enabling absorption without a permanent dipole moment. An engineering closed form is adopted and evaluated at frequency f (GHz) [7]; and a quantity N"_D(f) from total pressure p (hPa), water-vapour partial pressure e (hPa), and θ=300/T, then obtain:

$$\gamma_{\text{dry}}(f)\ [\text{dB/km}] = 0.1820\,f\,N''_D(f), \qquad \alpha_{\text{dry}}(f)\ [\text{m}^{-1}] = \frac{\gamma_{\text{dry}}}{4342.945}.$$

This term completes the non-aqueous background, independently of O_2 lines.

2.4. Frequency ↔ Wavenumber Conversions

With $c_0 = 2.99792458\times10^8$ m/s, the wavenumber [cm^{-1}] associated with f [GHz] is

$$\tilde{\nu} = \frac{f\cdot 10^9}{c_0\cdot 100}.$$

2.5. Transmission, FTS 3-GHz Binning, and Inversion

The total coefficient is:

$$\alpha_{\text{tot}}(f) = \alpha_{\text{lines}}(f) + \alpha_{\text{cont},H_2O}(f) + \alpha_{\text{dry}}(f).$$

High-resolution transmission over a path L:

$$T_{\text{HR}}(f) = \exp\left(-\alpha_{\text{tot}}(f)\,L\right).$$

FTS-style instrument binning in transmission over 3 GHz bands:

$$T_{\text{bin}}(k) = \langle T_{\text{HR}}(f)\rangle_{\text{bin}\,k}, \qquad \alpha_{\text{bin}}(k) = -\frac{\ln T_{\text{bin}}(k)}{L}.$$

The beamsplitter null region (≈ 748–756 GHz) and potential saturations are masked. The instrumental chain is explicitly replicated; Figure 4 details the HR computation, 3-GHz binning in transmission, inversion to α, and the pchip interpolation on the measurement axis.

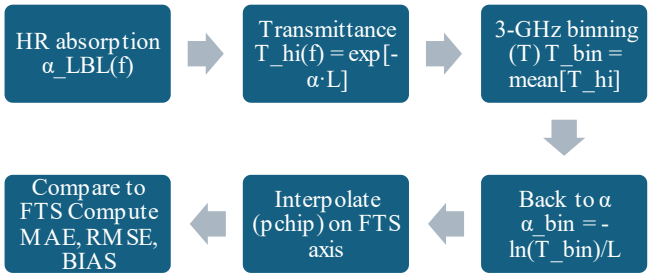

Fig. 4 Reproduced FTS processing chain

This alignment to the measurement workflow ensures that any residual is not a by-product of inconsistent processing.

2.6. FTS Measurement Axis and Metrics

Binned curves are interpolated (pchip) onto the FTS measurement axis. The metrics are:

$$\text{MAE} = \text{mean}|\alpha_{\text{mod}} - \alpha_{\text{mes}}|, \quad \text{RMSE} = \sqrt{\text{mean}(\alpha_{\text{mod}} - \alpha_{\text{mes}})^2},$$
$$\text{MAXE} = \max|\alpha_{\text{mod}} - \alpha_{\text{mes}}|, \quad \text{BIAIS} = \text{mean}(\alpha_{\text{mod}} - \alpha_{\text{mes}}),$$

Reported over 300–1000 GHz and by windows (e.g., Z4: 640–710 GHz; Z5: 800–900 GHz).

2.7. Spectral Factor S(f) (Integrated into the LBL, Foreign-Only, Windowed, Guard-Railed)

To reconcile the observed valley background without modifying the micro-physics of lines or the self-component, a factor is integrated:

$$S_{\text{lin}}(f) = A + B\,f \quad (\text{GHz}), \qquad S_{\text{eff}}(f) = 1 + \gamma\,[S_{\text{lin}}(f) - 1]\,W(f).$$

The smoothed window W(f) restricts action to [600, 720, 930, 980] GHz. Bounds (min/max gain) prevent any drift. The update applies only to

$$\alpha_{\text{foreign}}(f) \leftarrow S_{\text{eff}}(f)\,\alpha_{\text{foreign}}(f),$$

While α_lines, α_self, and α_dry remain unchanged. Guardrail (local): apply S_eff only if the foreign fraction dominates the continuum,

$$F_{\text{foreign}}(f) = \frac{\alpha_{\text{foreign}}}{\alpha_{\text{self}} + \alpha_{\text{foreign}}} \geq 0.60.$$

Parameters used: A = 3.7830, B = −0.001206, γ = 0.60.

The affine trend S(f) = A + Bf is determined by a least-squares fit on the valley residuals (Z4 ∪ Z5) aggregated over the four FTS cases, where residuals are α_LBL − α_FTS on the measurement axis. The global amplitude γ is then selected by leave-one-case-out cross-validation: for each held-out humidity case, γ minimizes MAE_Z4 + MAE_Z5 computed on the remaining three cases, and performance is reported on the held-out case. The raised-cosine window [f0, f1, f2, f3] = [600, 720, 930, 980] GHz and the guard condition F_foreign ≥ 0.60 are kept fixed by design, so that scaling is applied only where the foreign continuum both dominates and matters. This

procedure yields a stable optimum around $\gamma \approx 0.60$ and avoids over-tuning to any single humidity case. The fraction of HR points is also reported within the window where the guard is active (coverage), as an additional sanity check.

2.8. Constants, Parameters, and Numerical Chain

Constants: $c_0 = 2.99792458 \times 10^8$ m/s, $c_2 = hc/k$, $R_v = 461.5\ \mathrm{J\,kg^{-1}\,K^{-1}}$.

Conversions : $\tilde{\nu}[\mathrm{cm^{-1}}] = (f \cdot 10^9)/(c_0 \cdot 100)$; $\mathrm{Np/cm} \rightarrow \mathrm{dB/km} : 10\log_{10} e \times 10^5$;

Chain: HR calculation → α_tot → T = exp (−α L) → 3-GHz binning in T (FTS protocol chosen for validation) → α = −ln T/L → instrument masks → pchip interpolation to the measurement axis → metrics.

3. Results and Discussion

3.1. FTS Validation Framework and Computing Environment

This approach is validated on the FTS experiment by Slocum et al.: cell ≈ 4 m, T≈296 K, P≈1 atm, band 300–1000 GHz and four humidity levels. The cases used in the MATLAB scripts correspond to water densities: Case #1 ρw≈3.51 g/m³, Case #2 ρw≈7.85 g/m³, Case #3 ρw≈9.81 g/m³, Case #4 ρw≈14.86 g/m³. To match the instrumental protocol, the FTS chain is reproduced: high-resolution calculation, 3-GHz transmission binning, return to α via −ln T/L, then pchip interpolation onto the FTS measurement axis. All steps (LBL, HITRAN/NetCDF reading, exact Voigt/Faddeeva, MT_CKD 4.3 self/foreign, dry CIA, binning, metrics) are implemented in MATLAB.

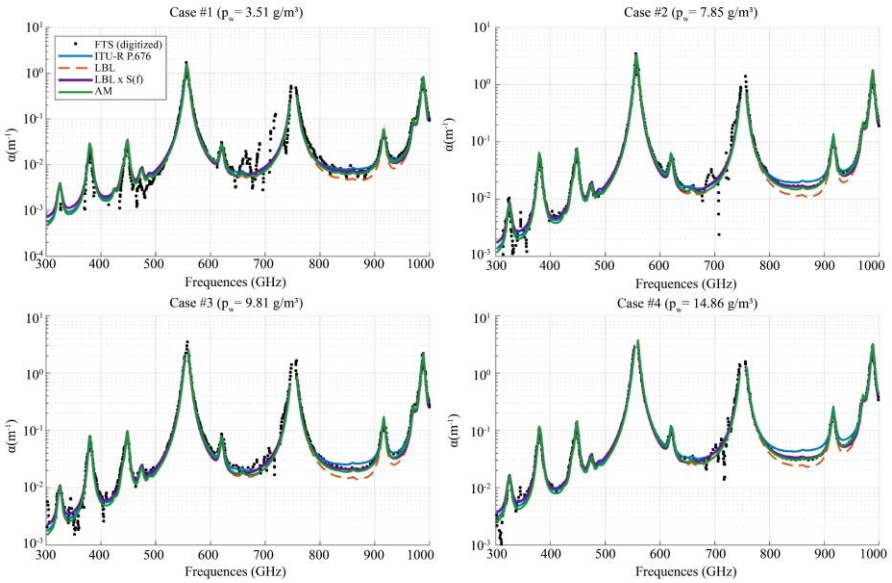

Fig. 5 Global comparison (300–1000 GHz): FTS vs LBL, LBL×S(f), ITU-R P.676, and AM (Cases #1–#4)

Figure 5 compares the four humidity cases over 0.3–1 THz. The bare LBL tracks the peaks but sits low in valleys; LBL×S(f) lifts the background without touching peaks; ITU-R P.676 trends higher overall; AM stays close on average but shows residual underestimation in some valleys.

3.2. Metrics and the Role of Bias

MAE, RMSE, BIAS (defined as BIAS = ⟨αmod − αmeas⟩) and MAXE are reported. Bias is the natural metric to quantify a systematic drift (model too high/too low); it is always interpreted together with MAE/RMSE (error amplitudes). This triplet is standard in spectroscopic validation and perfectly suited here, since S(f) aims to correct a localized background offset.

3.3. Global Reading (300–1000 GHz)

Across the full band, the uncorrected LBL model tracks the measured data closely and typically falls between the AM and ITU curves. Broadly speaking, ITU tends to show a slight positive bias, AM remains nearly unbiased overall but can dip slightly below in certain valley regions, and the bare LBL exhibits a small overall bias, with a noticeable background shortfall in zones Z4 and Z5 depending on humidity.

This pattern points to the need for a selective adjustment focused on the H_2O–air continuum (foreign component), while leaving the line contributions and the self-broadened term untouched. That is exactly the role of the frequency-dependent scaling function S(f), which is integrated into the LBL framework as detailed in Section 2.

3.4. Effect of S(f) (Foreign-Only, Windowed): Summary by Table

In what follows, "Before" = LBL + dry CIA, "After" = LBL×S(f) + dry CIA. Z4 = [640–710] GHz; Z5 = [800–900] GHz. Values are in m^{-1}.

Table 3.1. Effect of S(f) on MAE and BIAS

Case (ρw)	Region	MAE Before	MAE After	ΔMAE (%)	BIAS Before	BIAS After	ΔBIAS
#1 (≈3.51)	Global	0.021849	0.021427	+1.9	−0.002330	−0.001545	+0.000785
	Z4	0.006032	0.005663	+6.1	−0.005113	−0.004063	+0.001050
	Z5	0.002671	0.001219	+54.4	−0.002671	−0.000373	+0.002298
#2 (≈7.85)	Global	0.036603	0.035524	+2.9	+0.000221	+0.001659	+0.001438
	Z4	0.006391	0.005920	+7.4	−0.001961	+0.000764	+0.002725
	Z5	0.005398	0.000514	+90.5	−0.005398	−0.000265	+0.005133
#3 (≈9.81)	Global	0.043359	0.042055	+3.0	−0.024487	−0.022652	+0.001835
	Z4	0.007011	0.004778	+31.9	−0.006731	−0.003359	+0.003371
	Z5	0.008127	0.001928	+76.3	−0.008127	−0.001752	+0.006375
#4 (≈14.86)	Global	0.044929	0.044041	+2.0	+0.000588	+0.003473	+0.002885
	Z4	0.006546	0.006533	+0.2	−0.003174	+0.002209	+0.005383
	Z5	0.007719	0.002160	+72.0	−0.007719	+0.001921	+0.009640

Over the whole band, MAE gains remain modest (+2–3 %), which is consistent with the intention: not to affect the peaks (micro-physics of lines intact). — Valleys: Z5 systematically benefits from the strongest gains (+54–91 % MAE); Z4 improves more moderately (0–32 %). — Bias: the negative drift of the bare LBL in valleys is strongly attenuated.

In Z4, a slight positive can appear (Cases #2 and #4), of small amplitude (~10^{-3} m^{-1}), consistent with the chosen compromise (γ=0.60) that maximizes Z5 while keeping Z4 reasonable.

3.5. Comparison with References (ITU-R P.676, AM)

Across all four humidity scenarios, ITU-R P.676 consistently maintains a positive bias, while AM remains nearly unbiased overall but still shows some residual mismatches in valley regions. In contrast, the proposed LBL×S(f) model applies a focused correction to valleys—specifically in zones Z4 and Z5—without altering the spectral peaks. As a result, it remains unobtrusive across the broader band while delivering improvements precisely where they matter most for THz link design.

3.6. Role of the "dry" Background (CIA N_2/O_2)

Under these FTS conditions, the dry CIA remains far smaller than the water continuum in valleys; it does not explain the background deficit observed with the uncorrected LBL and does not change the conclusions on S(f).

Figure 6 quantifies the valley means of dry CIA relative to the H_2O continuum for all four cases.

The dry contribution is minor here (< 1 % of the valley residual explained); It stays orders of magnitude lower than the water continuum under these FTS conditions, confirming it cannot explain the observed valley offset.

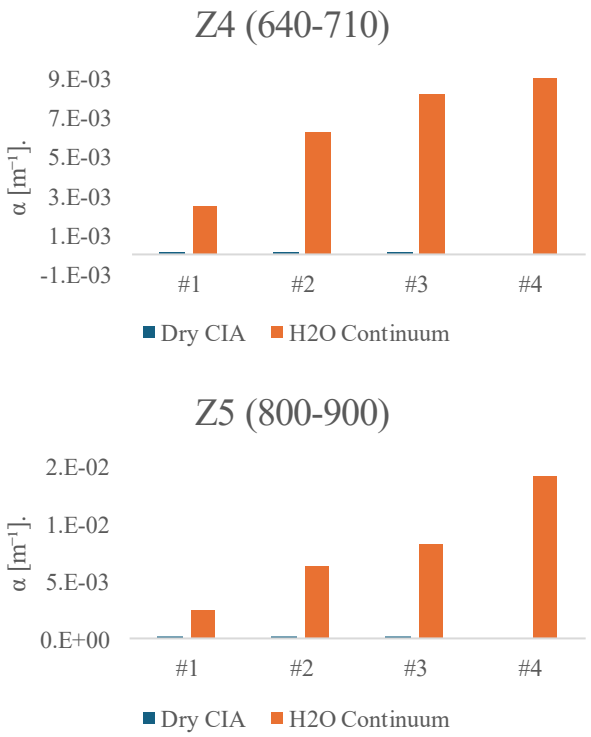

Fig. 6 Dry CIA vs H_2O continuum (valley means Z4/Z5, cases #1–#4)

3.7. Link-Budget Implications

In a link, the specific loss γ in dB/km is obtained by γ [dB/km] ≈ 4342.945 × α [m^{-1}]. Thus, a 10^{-3} m^{-1} bias corresponds to ≈ 4.34 dB/km of systematic error on gaseous attenuation. The bias corrections brought by S(f) in valleys, therefore, translate into tens of dB/km "re-allocated", which concretely changes the link margin (SNR, range, modulation scheme). Numerical examples from the runs:

- Case #3, Z5: Δbias = +0.006375 m^{-1} ⇒ ≈ 27.7 dB/km better centered.

- Case #2, Z5: Δbias = +0.005133 m^{-1} ⇒ ≈ 22.3 dB/km;
- Case #4, Z5: Δbias = +0.009640 m^{-1} ⇒ ≈ 41.9 dB/km;
- Case #1, Z5: Δbias = +0.002298 m^{-1} ⇒ ≈ 10.0 dB/km.

Although the overall improvement across the full 300–1000 GHz band remains modest—as intended—the background correction brings clear benefits within the usable spectral windows. It helps avoid underestimating path loss, which could lead to overly optimistic range predictions due to a negatively biased model and overestimating required margins if the model is biased high. By applying a calibrated, decomposable LBL adjustment through S(f), more reliable loss estimates are obtained—essential for planning choices like window selection, link distance, expected throughput, and margin budgeting for fading or weather. Figure 7 illustrates the affine windowed form used for the foreign-component scaling (γ = 0.60; [600, 720, 930, 980] GHz), with unity gain applied outside the correction range.

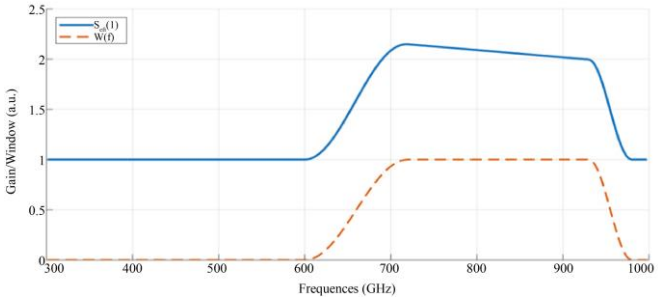

Fig. 7 Effective scaling S(f) and W(f): action range and bounds

As designed, the overall MAE gain across the full band remains modest—since spectral peaks are deliberately left untouched—while valley-specific metrics show strong improvement wherever W(f)=1. This aligns with the methodological intent described earlier. Peaks preserved; floor lifted. The scaling function specifically targets the valley floor, leaving peak regions unaffected: at the centers of strong HITRAN lines within the [600–980] GHz range, the model difference $\Delta\alpha(f) = \alpha\_\{LBL\times S\} - \alpha\_\{LBL\}$ stays close to zero, with no observable broadening or change in peak height. The performance gain clearly results from elevating the inter-line background, not from modifying the resonant features. This behavior holds consistently across all four humidity cases and explains the significant error reduction in Z5, despite only modest MAE change when averaged over the entire band.

3.8. Scientific Neutrality and Limitations

S(f) is presented as a built-in calibration lever within the LBL framework, specifically tailored to the 0.3–1 THz range and the FTS conditions considered here, not as a universal physical truth. Its design is intentionally simple: an affine function, windowed, bounded, and protected by a foreign-dominance threshold to prevent use outside its intended context. That said, there are limitations to note—chiefly, the reliance on a single FTS dataset (Slocum et al.) and the validation based on digitized FTS figures, which introduces a small but non-negligible degree of uncertainty. Looking ahead, broader validation—using other FTS data, radiative models like LBLRTM, or different temperature, pressure, and humidity conditions—will be essential to consolidate further or refine S(f), and to explore variations in parameters like γ or the window boundaries. Still, such refinements are unlikely to change the main conclusion observed here: zone Z5 consistently shows the greatest benefit.

4. Conclusion

A decomposable line-by-line (LBL) model is developed over the 0.3–1 THz range that explicitly separates the physical contributions from spectral lines (via HITRAN, using exact Voigt profiles computed with the Faddeeva function), the continuum components (MT_CKD 4.3, with self and foreign terms handled independently), and the dry-air background due to collision-induced absorption (CIA from N_2/O_2). The numerical workflow closely reproduces the reference FTS protocol in MATLAB, enabling a direct comparison with experimental data. This framework serves as a simulation tool and an explanatory model that links individual physical mechanisms to the observed attenuation patterns.

During validation, the uncorrected LBL model revealed a consistent background shortfall in specific valley regions, while peak features remained accurate and stable. To address this, a selective and constrained correction that targets only the foreign-broadened continuum is introduced: a scaling factor S(f) designed to be affine and windowed (600–980 GHz), damped (γ = 0.60), and bounded by a foreign-dominance threshold to avoid misuse. Notably, the spectral lines and the self-component are left untouched.

The results align with the design goal: a modest improvement over the full band (MAE reduction of 2–3%), paired with a more significant correction within valley regions—most notably in Z5 (800–900 GHz), where both the mean error and spectral drift are clearly reduced. In Z4 (640–710 GHz), the improvement is more moderate, and a slight positive bias of limited amplitude may appear—an acceptable trade-off that favors stability and improvement in the more critical Z5 range. Under the test conditions, the dry-air CIA remains negligible relative to the H_2O contribution and does not account for the observed baseline mismatch. Compared to aggregated models such as ITU-R P.676 or AM, the LBL×S(f) correction recenters the background level precisely where it impacts link design most.

S(f) is not proposed as a universal law, but rather as a calibrated lever integrated into the LBL under specific experimental conditions—used only when the data reveal a localized background discrepancy. Its simple, bounded, and windowed form is intentionally constructed to minimize out-of-domain drift or overreach. Future work will focus on broader validation—using additional FTS datasets, running

comparisons with LBLRTM under equivalent conditions, and exploring the impact of temperature, pressure, and humidity variations. These efforts may help refine the shape of S(f) while keeping complexity constant (e.g., tuning γ or adjusting window boundaries). They will support the integration of LBL×S(f) into a THz link simulator to evaluate planning scenarios under diverse weather conditions.

In short, this work contributes on two fronts: first, by proposing a decomposable LBL model that restores physical transparency to attenuation modeling; and second, by introducing a measured calibration of the foreign continuum that improves valley alignment without disturbing the lines. Together, these steps lay the groundwork for a more reliable and controlled link-budget framework in future THz communication systems.

References

[1] Recommendation ITU-R P.676-13, Attenuation by Atmospheric Gases and Related Effects, International Telecommunication Union, Geneva, 2022. [Publisher Link]

[2] Scott Paine, "The am Atmospheric Model," *Submillimeter Area Technical Memo*, 2019. [CrossRef] [Publisher Link]

[3] David M. Slocum et al., "Atmospheric Absorption of Terahertz Radiation and Water Vapor Continuum Effects," *Journal of Quantitative Spectroscopy and Radiative Transfer*, vol. 127, pp. 49-63, 2013. [CrossRef] [Google Scholar] [Publisher Link]

[4] I.E. Gordon et al., "The HITRAN2020 Molecular Spectroscopic Database," *Journal of Quantitative Spectroscopy and Radiative Transfer*, vol. 277, pp. 1-82, 2022. [CrossRef] [Google Scholar] [Publisher Link]

[5] Franz Schreier, "The Voigt and Complex Error Function: Humlíček's Rational Approximations Revisited," *Monthly Notices of the Royal Astronomical Society*, vol. 479, no. 3, pp. 3068-3075, 2018. [CrossRef] [Google Scholar] [Publisher Link]

[6] AER Radiation & Climate / MT_CKD_H2O, MT_CKD Water Vapor Continuum Model (Code and NetCDF), GitHub Repository, 2025. [Publisher Link]

[7] Tijs Karman et al., "Update of the HITRAN Collision-Induced Absorption Section," *Icarus*, vol. 328, pp. 160-175, 2019. [CrossRef] [Google Scholar] [Publisher Link]